



HAL
open science

Electrochemical Impedance Spectroscopy of PEO-LATP Model Multilayers: Ionic Charge Transport and Transfer

James Alfred Isaac, Léa Rose Mangani, Didier Devaux, Renaud Bouchet

► To cite this version:

James Alfred Isaac, Léa Rose Mangani, Didier Devaux, Renaud Bouchet. Electrochemical Impedance Spectroscopy of PEO-LATP Model Multilayers: Ionic Charge Transport and Transfer. ACS Applied Materials & Interfaces, 2022, 10.1021/acsami.1c19235 . hal-03631162

HAL Id: hal-03631162

<https://hal.science/hal-03631162>

Submitted on 5 Apr 2022

HAL is a multi-disciplinary open access archive for the deposit and dissemination of scientific research documents, whether they are published or not. The documents may come from teaching and research institutions in France or abroad, or from public or private research centers.

L'archive ouverte pluridisciplinaire **HAL**, est destinée au dépôt et à la diffusion de documents scientifiques de niveau recherche, publiés ou non, émanant des établissements d'enseignement et de recherche français ou étrangers, des laboratoires publics ou privés.

Electrochemical Impedance Spectroscopy of PEO-LATP Model Multilayers: Ionic Charge Transport and Transfer

James Alfred Isaac,[‡] Léa Rose Mangani,[‡] Didier Devaux, and Renaud Bouchet*Cite This: *ACS Appl. Mater. Interfaces* 2022, 14, 13158–13168

Read Online

ACCESS |



Metrics & More



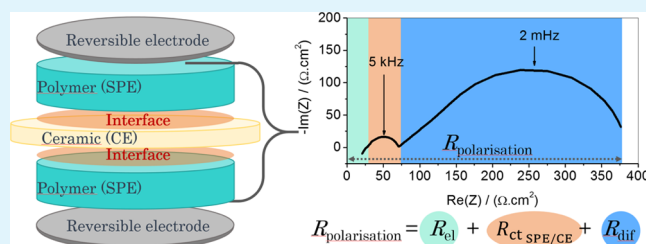
Article Recommendations



Supporting Information

ABSTRACT: Solid-state batteries are seen as a possible revolutionary technology, with increased safety and energy density compared to their liquid-electrolyte-based counterparts. Composite polymer/ceramic electrolytes are candidates of interest to develop a reliable solid-state battery due to the potential synergy between the organic (softness ensuring good interfaces) and inorganic (high ionic transport) material properties. Multilayers made of a polymer/ceramic/polymer assembly are model composite electrolytes to investigate ionic charge transport and transfer. Here, multilayer systems are thoroughly studied by electrochemical impedance spectroscopy (EIS) using poly(ethylene oxide) (PEO)-based polymer electrolytes and a NaSICON-based ceramic electrolyte. The EIS methodology allows the decomposition of the total polarization resistance (R_p) of the multilayer cell as being the sum of bulk electrolyte (migration, R_{el}), interfacial charge transfer (R_{ct}), and diffusion resistance (R_{dif}), i.e., $R_p = R_{el} + R_{ct} + R_{dif}$. The phenomena associated with R_{el} , R_{ct} , and R_{dif} are well decoupled in frequencies, and none of the contributions is blocking for ionic transport. In addition, straightforward models to deduce R_{el} , R_{dif} , and t^+ (cationic transference number) of the multilayer based on the transport properties of the polymer and ceramic electrolytes are proposed. A kinetic model based on the Butler–Volmer framework is also presented to model R_{ct} and its dependency with the polymer electrolyte salt concentration (C_{Li^+}). Interestingly, the polymer/ceramic interfacial capacitance is found to be independent of C_{Li^+} .

KEYWORDS: impedance spectroscopy, polymer/ceramic electrolyte interfaces, solid-state electrolytes, polymer electrolytes, lithium batteries



INTRODUCTION

With our increasing demand for carbon-free renewable energy, the development of high-energy-density and safe batteries is key. Lithium (Li) metal has been identified as the ultimate negative electrode due to its particularly high gravimetric capacity (3.86 A·h/g) and low potential (−3.04 V vs SHE, standard hydrogen electrode), which are the two levers to increase the energy density in an electrochemical generator.^{1–3} However, Li is known to form dendrites when the battery is recharged, which eventually short-circuit the device and lead to hazard issues (fire, explosion). Many solutions to prevent dendrite nucleation and growth have been proposed, such as using a nonflammable solid separator⁴ or forming a stable solid electrolyte interphase (SEI) at the Li/electrolyte interface.^{5–7} One strategy aims then at developing all-solid-state Li metal batteries,^{8,9} which could mitigate dendrite growth and increase both battery safety and cycle life.

Solid-state electrolytes fall into two major classes: organic polymers and inorganic ceramics. Solid polymer electrolytes (SPEs) have significant advantages in terms of their mechanical properties, as they develop excellent contacts with electrodes and withstand battery volume changes due to their plasticity. However, their low ionic conductivity at room temperature (typically 10^{-5} S/cm) hinders their practical use.^{10,11} In

addition, adding polar solvents to form gels dramatically increases their conductivity leading to batteries operating at temperatures close to room temperature but to the detriment of both the safety and their required mechanical properties.^{10,12} Conversely, ceramic electrolytes (CE) are advantageous in terms of thermostability and ionic conductivity, with NaSICONs, garnet-type structures, and sulfide-based materials reaching a conductivity of 10^{-4} – 10^{-3} S/cm at room temperature.^{13,14} However, the mechanical properties of ceramics are far from ideal compared to SPEs due to their brittle nature, preventing smooth and intimate contact at electrode–electrolyte interfaces, and the assembly of flexible commercial batteries.

Composite electrolytes have therefore come to light as an elegant solution comprising the mechanical properties of SPEs and the high ionic conductivity of CEs. The addition of nonconducting ceramic particles (e.g., SiO_2 , Al_2O_3 , TiO_2) into

Received: October 6, 2021

Accepted: February 14, 2022

Published: March 8, 2022



SPEs can increase the overall conductivity of the composite SPE, especially at room temperature due to the mitigation of the polymer crystallinity, allowing Li^+ to easily transport through the amorphous matrix.^{15,16} The addition of Li^+ conducting ceramic particles (e.g., NaSICONs, garnets, etc.) to an ionically conducting polymer matrix can produce electrolytes that can operate at room temperature,¹⁷ but the role of the ceramic electrolyte is still unclear. Indeed, one would expect CE/polymer composites to reach a conductivity higher than composite electrolytes using nonconducting ceramic in SPE, but disparate results are reported.¹⁵ For example, Chen et al. reported an increase in conductivity upon addition of LLZTaO to a poly(ethylene oxide) (PEO) electrolyte (from 0.5×10^{-4} to 1.2×10^{-4} S/cm at 30 °C) up to 10 wt % followed by a decrease at a higher ceramic content,¹⁸ whereas other groups reported a continuous decrease in ionic conductivity upon the addition of a garnet to a PEO electrolyte.^{19,20} A high charge transfer resistance at the SPE/CE interface has been suggested as a possible explanation for the decrease in conductivity, so several groups have turned toward composites with an optimized structure,^{21–23} designed to limit the amount of polymer/ceramic interfaces a cation has to cross.²⁴ Indeed, the SPE/CE interface could add a significant resistance compared to that of the bulk electrolyte.^{25–27} Consequently, it is crucial to study SPE/CE/SPE model assemblies in an attempt to probe separately the contributions of ionic migration in the bulk and interfacial ionic charge transfer to determine their governing factors. More generally, the study of the ionic charge transfer mechanism occurring at the interface between a liquid electrolyte (LE) or an SPE and a solid Li^+ conductor by means of such a model cell can be extended to the electrode active material/electrolyte interface, following the approach of Ogumi et al.^{28–30} While at the electrolyte/electrode interface an electrochemical charge transfer reaction involving a mixed ionic/electronic exchange occurs, at the electrolyte/ceramic interface, an ionic charge transfer reaction takes place.

Significant advances have been made in elucidating the interface between liquid electrolytes and ceramic electrolytes.^{30–38} LE can be similar in their chemistry to polymers and can therefore give insight into factors that affect the SPE/CE interface. LE/CE interfaces have been thoroughly studied by Ogumi et al. using electrochemical impedance spectroscopy (EIS).^{30,31,38–41} Measurements using direct current have also been performed to further analyze the properties of the LE/CE interface.^{32,33,35} While the factors that affect the interfacial resistance are still unclear, a strong solvent–cation interaction in the LE seems to increase the interfacial resistance and activation energy,^{31,32,35,38,39} as the cation needs more energy to desolvate and transfer from the LE to the CE. Busche et al. also showed that a resistive interphase generally made of decomposition products of ceramic, solvent, and/or salt can negatively affect the LE/CE interfacial resistance.^{36,37,42} To understand the charge transfer kinetics at the interface between a LE made of LiPF_6 in a mixture of ethylene carbonate/dimethyl carbonate (EC/DMC) and a CE in LLZTaO, Schleutker et al. proposed a superposition of an ionic charge transfer process^{43–45} based on Butler–Volmer kinetics in series with an interphase resistance composed of degradation products.³²

In the literature, a few SPE/CE interfaces have been reported.^{40,46–56} As for the LE/CE interface studies, the activation energies and resistances obtained vary vastly

between groups. For example, the resistance of the interface between poly(ethylene oxide) (PEO) and NaSICON varies between 2.5 and 50 $\text{k}\Omega\cdot\text{cm}^2$ at 20 °C.^{46,50} Generally, measurements are made by impedance spectroscopy in a two-electrode cell as it is challenging to introduce reference electrodes within the thin SPE layers to make a four-electrode system. Nevertheless, independent of the electrode configuration, guaranteeing intimate contact in between each layer of material comprising the solid-state cell is a complicated task. Another difficulty impacting the interface resistance lies in the delicate interpretation of the impedance spectra in a two-electrode configuration due to (i) the choice of an adequate equivalent circuit that may vary from one publication to another^{50,57} and (ii) the overlap in frequencies of the electrode/SPE and SPE/CE interface contributions.²⁵ In the case of SPE/CE interfaces, to the best of our knowledge, only Brogioli et al.⁵⁷ reported a space charge layer model to describe the interfacial charge transfer reaction. The authors studied an SPE made of PEO/ LiClO_4 at different Li salt concentrations and a CE of LLZO. They interpreted the dielectric interfacial contribution within the framework of the Stern model,⁴³ where the SPE and LLZO domains are separated by the Stern layer. In addition, they assumed that the charge transfer is driven by a Butler–Volmer equation with a symmetry coefficient of 0.5. Similarly to the work of Schleutker et al.³² on the LE/CE interface, they reported that the interfacial resistance decreases with increasing salt concentration until a plateau value attributed to a space charge effect. Unfortunately, no data were provided for the evolution of the interface capacitance with the SPE salt concentration.

Herein, the transport properties through multilayer SPE/CE/SPE model cells are measured by EIS, using an LATP-type CE and PEO/lithium bis(trifluoromethane)sulfonimide (LiTFSI)-based SPE. A commercial cross-linked PEO-based electrolyte from Osaka Soda Co., Ltd⁵⁸ (OS) was used when a uniform thickness was needed and a 100 kg/mol PEO doped with LiTFSI was used to vary the salt concentration over a wide range of 1.0×10^{-2} to 2.5 M.⁵⁹ We provide a thorough electrochemical impedance analysis based on two-electrode cells comprising either blocking stainless steel (SS) electrodes or reversible Li electrodes to specifically probe the ionic charge transfer resistance at the CE/SPE interface as well as bulk and diffusion properties in a broad range of temperature from –30 to 100 °C. Impedance analysis of the SPE/CE/SPE cell showed that bulk (R_{el}), interfacial (R_{ct}) and diffusion contributions (R_{dif}) are well decoupled in the impedance spectra with different characteristic frequencies. Consequently, the SPE/CE/SPE overall polarization resistance given by $R_{\text{p}} = R_{\text{el}} + R_{\text{ct}} + R_{\text{dif}}$ can be determined by measuring each resistive contribution separately. Factors that pilot the bulk and the diffusion resistances of SPE/CE/SPE multilayers are fully determined, enabling prediction of apparent bulk ionic conductivity and apparent transference number. The SPE/CE interface is analyzed both in terms of resistance and capacitance. In addition, a kinetic model with minimal assumptions within the Butler–Volmer framework is proposed to depict the ionic exchange current density at the SPE/CE interface from which an expression of interfacial resistance is deduced, in agreement with the experimental data. This study, therefore, offers a full picture of a multilayer model system and present methodologies to extract the limiting factors at the SPE/CE interface. Such methodologies can then be applied to numerous SPE/CE systems.

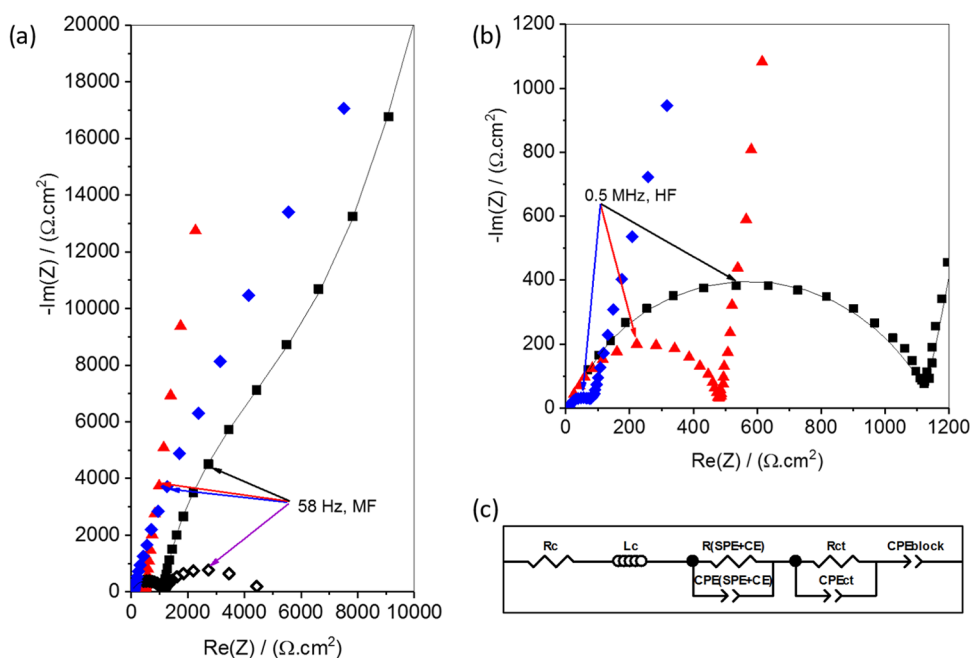


Figure 1. (a) Nyquist plots of the SS/OS/SS (red triangles), Au/Oh/Au (blue diamonds), and SS/OS/Oh/OS/SS (black squares) cells measured at 20 °C. In addition, the subtraction (black open diamonds) of the SS/OS capacitive contribution from the spectrum of SS/OS/Oh/OS/SS is also displayed. Markers: experimental values; solid line: fitted values, using the equivalence circuit displayed in (c). (b) Zoom on the HF region of the plot (a).

EXPERIMENTAL SECTION

Materials. All products were stored in an argon (Ar)-filled glovebox (H_2O , $\text{O}_2 < 1$ ppm, Jacomex) and used as received. Ceramic plates (Oh) were purchased from Ohara Corp.⁶⁰ in the form of one-inch squared plates with thicknesses of 50 or 150 μm . The ceramic is similar to LATP with the main crystalline phase being $\text{Li}_{1+x+y}\text{Al}_x\text{Ti}_{2-x}\text{Si}_y\text{P}_{3-y}\text{O}_{12}$, but the exact chemical nature is the property of the company. A 49 μm thick SPE film (named OS in this paper) based on a cross-linked polyethylene oxide (PEO) was purchased from Osaka Soda Co., Ltd. In addition, PEO/LiTFSI electrolytes were formulated using a solvent-free method: the relevant amounts of lithium bis(trifluoromethane)sulfonimide (LiTFSI, Solvay) and PEO 100 kg/mol (Alfa Aesar) were first cold-mixed by hand and then heated to 80 °C for at least 4 h in the Ar-filled glovebox (H_2O , $\text{O}_2 < 1$ ppm, Jacomex) while being frequently stirred until a homogeneous mixture is obtained. Finally, the resulting mixture was hot-pressed at 70 °C, still in the glovebox, to form the electrolyte membrane. To confirm the exact Li salt concentration in the polymer membrane, inductively coupled plasma mass spectroscopy (ICP-MS, PerkinElmer NexION 2000c) was used (see the Supporting Information, SI, for details). For simplicity, the PEO/LiTFSI electrolytes are denoted PEO/LiTFSI- $x\text{M}$, with x being the LiTFSI salt concentration ranging from 1.0×10^{-2} M (EO/Li = 2500) to 2.5 M (EO/Li = 7) and are also listed in Table S1.

Cell Assembly. All cells were assembled in the glovebox. To study the interface between the SPE (OS or PEO/LiTFSI- $x\text{M}$) and the Oh ceramic, symmetrical CR2032 coin cells comprising stainless steel (SS) blocking electrodes or Li metal were used. For SS symmetric cell assembly, a PEO/LiTFSI- $x\text{M}$ film was flowed directly within a spacer defining a 10 mm active diameter onto a 16 mm diameter SS electrode using a hot press (Specac) to get an intimate contact. A similar procedure was performed again to form a second SPE/SS element. Then, a piece of Oh ceramic with sides longer than the spacer inner diameter was placed between the two SPE/SS elements by gently pressing them altogether prior to closing the coin cell with a crimper. For Li symmetric cells, the assembly procedure is similar to that of the blocking electrodes except that, beforehand, an SPE layer and an 8 mm diameter Li electrode are laminated together at 80 °C and 3 bar. For OS as the SPE, a similar procedure was used but by

manually pressing the cross-linked polymer against the SS electrode instead of flowing the polymer with a hot press. The cells are denoted Li/SPE/Oh/SPE/Li or SS/SPE/Oh/SPE/SS depending on the cell assembly and SPE nature (OS or PEO/LiTFSI- $x\text{M}$). In addition, Li/SPE/Li and SS/SPE/SS symmetric cells were also assembled to study the Li/SPE interface and the bulk SPE contributions separately. Finally, the conductivity of the ceramics Oh was measured in Swagelok-type cells in which the surface of the ceramic was coated by gold sputtering (of known surface area) to ensure good electrical contacts with the current collectors. This last cell is denoted Au/Oh/Au.

Impedance Measurements. After assembly, the cells were taken out of the glovebox, placed in a climatic chamber (Clima Temperatur Systeme), and connected to a multipotentiostat with impedance capabilities (VMP300, BioLogic). Electrochemical impedance spectroscopy (EIS) was performed in the frequency range of 7 MHz down to 0.1 Hz (and 100 μHz for reversible Li/Li-based cells) using an excitation voltage between 10 and 200 mV depending on the impedance of the cell. The use of high excitation signal enabled the reduction of noise for the large impedance measurements especially when the temperature was low; however, the linearity of the impedance answer was always checked. When OS was used as the SPE, the chamber temperature was varied from -30 to 100 °C with a temperature program by 10 °C steps as follows: (i) heat from room temperature to 100 °C, (ii) cool to -30 °C and (iii) finally heat to 100 °C. With PEO/LiTFSI- $x\text{M}$ as the SPE, the same sequence was used in between 10 and 100 °C with temperature steps of 5 °C between 60 and 100 °C, where the PEO is in a melted state, and steps of 10 °C below 60 °C. EIS spectra were recorded after temperature stabilization of the cells, i.e., when the EIS spectra reach a steady state. The temperature was measured with a thermocouple type k located close to the cells.

METHODOLOGIES, RESULTS, AND DISCUSSION

EIS Data Treatment. Figure 1a displays the typical EIS spectra obtained at 20 °C in Nyquist coordinates of symmetric cells with blocking electrodes for the two reference cells SS/OS/SS and Au/Oh/Au as well as the multilayer SS/OS/Oh/

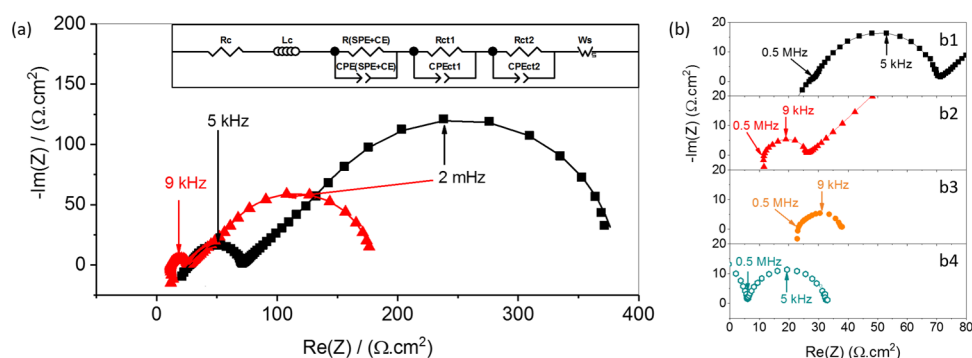


Figure 2. (a) Nyquist plots of the cells Li/OS/Li (red triangles) and Li/OS/Oh/OS/Li (black squares) measured at 80 °C between 7 MHz and 0.2 mHz. The lines are the results of the fit using the equivalent circuit displayed in the inset. (b) Series of spectra detailing the difference methodology with (b1) HF and MF zoom for Li/OS/Oh/OS/Li, (b2) Li/OS/Li, (b3) simulated Li/OS/OS/Li in the HF and MF range, and (b4) the result of the difference between Li/OS/Oh/OS/Li (b1) and Li/OS/OS/Li (b3) in the HF and MF range.

OS/SS cell, while Figure 1b is a zoom on the high-frequency (HF) domain. The bode plot at 20 °C and the spectra of the same cells at 80 °C are displayed in Figures S1 and S2, respectively. As expected for the two reference cells, the spectra are composed of the HF bulk electrolyte response (modeled by R_{oh}/CPE_{oh} (a resistance R in parallel with a constant phase element CPE) or R_{os}/CPE_{os}) superimposed with the cable contribution [resistance (R_c) and inductance (L_c)], followed at low frequency (LF) by the capacitive behavior due to the charge accumulation at the blocking SS electrode surface (modeled by CPE_{block}) as no charge transfer reaction is possible. For the multilayer cell, in addition to the HF bulk electrolytes contribution and the LF frequency capacitive behavior, there is a medium-frequency (MF) contribution (at around 60 Hz) superimposed with the beginning of the capacitive behavior. To visualize the contribution of the OS/Oh interface without the overlapping capacitive response, the LF part of the SS/OS/SS spectra (assigned to the SS/OS capacitive response) is subtracted from the spectrum of the SS/OS/Oh/OS/SS cell, and the result is added in Figure 1a. A clear loop appears at MF with a characteristic frequency of 58 Hz, which demonstrates that a simple circuit made of a resistance in parallel with a constant phase element is correct to model the CE/SPE interfacial contribution. Therefore, the electrical equivalent circuit presented in Figure 1c that takes into account the HF, MF, and LF contributions is used to fit the multilayer cell impedance spectra. The result of the fit ($\chi^2 > 0.99$) of the SS/OS/Oh/OS/SS spectrum, added in Figure 1a,b, is in very good agreement with the experimental data. However, to get insight into the intricacies of the bulk electrolyte properties with the interfacial contributions that are still under debate in the literature,^{42,57,61} cells with reversible Li electrodes were also investigated. Indeed, Li electrodes allow charge transfer reactions between the electrolyte and the Li enabling measurement of diffusion properties in the LF range.^{30,31,54,62} Typically, to probe the diffusion contribution in an acceptable frequency range, higher than 0.1 mHz, a high temperature is preferred to increase the characteristic frequency of the thermally activated finite-length diffusion contribution.

Figure 2a,b presents typical EIS spectra recorded at 80 °C for the cells Li/OS/Oh/OS/Li and Li/OS/Li. For completeness, the spectra of the same cells at 20 °C are also shown in Figure S3. The spectra are divided into three frequency domains (HF, MF, and LF). For the Li/OS/Li spectrum, the

HF, MF, and LF contributions are, respectively, assigned to the OS bulk electrolyte response, the Li/OS interface response mainly due to the solid electrolyte interphase (SEI) with a characteristic frequency of 9 kHz, and the diffusion process within the SPE with a 2 mHz characteristic frequency located at the apex of the short Warburg loop.⁶² The HF contribution is distorted by the inductive behavior of the electric cables connecting the cell to the impedance meter, and at this temperature, mainly the resistive behavior of the bulk electrolyte is seen. For the Li/OS/Oh/OS/Li cell, the spectrum is similar to the reference Li/OS/Li cell but with bigger contributions in each frequency domain (HF, MF, LF). Indeed, the HF resistance contains bulk contributions from both the two SPE layers and the CE. The MF semicircle presents a characteristic frequency of 5 kHz close to that of the MF loop in the Li/OS/Li cell, and finally, at LF, a characteristic limited-length diffusion loop is observed with a similar characteristic frequency to that of the Li/OS/Li. It is clear here that the contribution of the CE/SPE interface is buried in the large MF loop, which illustrates the delicateness of data analysis when reversible electrodes are used.^{30,31,36,54}

To extract meaningful physical information on the interfaces from the spectra of the multilayer Li symmetric cell, we used a difference methodology depicted in Figure 2b. First, a theoretical Li/OS/OS/Li spectrum shown in Figure 2b3 limited to the HF and MF range (without the diffusion process) is simulated by doubling the HF contributions ($Re(Z)$ and $-Im(Z)$) of the Li/OS/Li cell spectrum (Figure 2b2), which leads to the shift of its MF loop by a constant value corresponding to R_{os} . Then, this simulated spectrum is subtracted from the experimental one of Li/OS/Oh/OS/Li (Figure 2b1) resulting in the spectrum shown in Figure 2b4. Interestingly in this difference spectrum, at high temperatures, the HF contribution perfectly fits the Oh electrolyte behavior (see Figure S4 for the Arrhenius plot), followed by an MF loop assigned to the OS/Oh interface. Therefore, this methodology allows the separation of all of the bulk and interfacial contributions between the Li, SPE, and the CE.

Results Obtained for Each Frequency Domain. We now focus on each contribution to detail the behavior of the multilayer cell at equilibrium. For the HF loop, the associated resistance is used to calculate the effective ionic conductivities (σ_{eff}) in between -30 and 100 °C. Figure 3 represents σ of Oh, OS, and the sandwich OS/Oh/OS as a function of the inverse of the temperature. The ceramic electrolyte (Oh) displays a

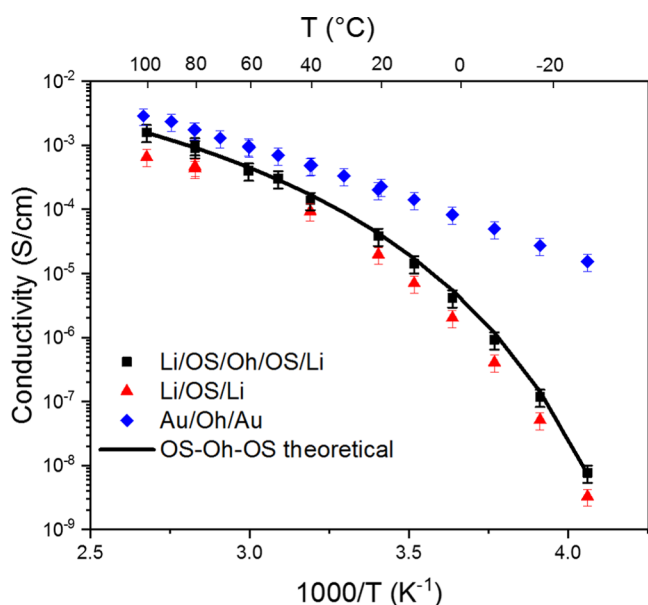


Figure 3. Arrhenius plot of the conductivities (high-frequency contribution) of electrolytes OS (red triangles) and Oh (blue diamonds) and the sandwich OS/Oh/OS (black squares) along with the theoretical values of OS/Oh/OS (black line) using eq 1.

typical Arrhenius-type behavior, with a conductivity of $2.2 \pm 0.2 \times 10^{-4}$ S/cm at 25 °C and an activation energy of 0.31 eV, both values being in very good agreement with the producer's values. Concerning the polymer electrolyte OS, the conductivity–temperature relationship follows a typical Vogel–Tammann–Fulcher⁶³ (VTF) behavior (see Figure S5 and Table S2 for fitting, with T_g experimentally determined by differential scanning calorimetry (DSC) in Figure S6). The SPE conductivity is always lower than that of the CE with a difference being amplified as the temperature is lowered with a factor of 1000 at –30 °C. Interestingly, the conductivity of the multilayer OS/Oh/OS lies in between the ones of OS and Oh. By considering that the overall resistance of the OS/Oh/OS multilayer is simply the sum of each layer resistances, a theoretical conductivity (σ^{Theo}) can be calculated from each independent conductivity measurement of the OS (σ_{OS}) and Oh (σ_{Oh}) following eq 1

$$\sigma^{\text{Theo}} = \frac{2l_{\text{OS}} + l_{\text{Oh}}}{\frac{2l_{\text{OS}}}{\sigma_{\text{OS}}} + \frac{l_{\text{Oh}}}{\sigma_{\text{Oh}}}} \quad (1)$$

where l_{Oh} and l_{OS} are the thicknesses of the OS and Oh electrolyte layers, respectively.

The values of σ^{Theo} of the OS/Oh/OS multilayer electrolyte are added as a continuous line in Figure 3. It fits almost perfectly the experimental σ_{eff} values of the Li/OS/Oh/OS/Li cell, showing that the resistances of the OS and Oh electrolytes are purely additive and that the OS/Oh interface does not limit the overall ionic transport. In addition, this result confirms intimate contacts between the organic and inorganic components in the multilayer system.

Note, for a battery application operating at room temperature, eq 1 applied on a realistic multilayer made of 2 thin SPE layers (typically 1 μm thick each with $\sigma_{\text{SPE}} \sim 10^{-5}$ S/cm) surrounding a thicker CE (typically 20 μm thick with $\sigma_{\text{CE}} \sim 4 \times 10^{-4}$ S/cm) leads to an effective conductivity (1.7×10^{-4} S/cm) higher than the target value (10^{-4} S/cm) needed for solid-

state battery cycling. In addition, the investigation of PEO/LiTFSI- x M/Oh systems with x spanning over almost 3 decades, from 10 mM to 2.5 M (equivalent to a range of EO/Li from 7 to 2500) as reported in Figure S8c, also demonstrates that the PEO/LiTFSI and Oh resistances are additive.

To further probe the transport properties, the LF loops of the OS/Oh/OS multilayer and the OS electrolyte (see Figure 2a) spectra are analyzed, as they present a typical short Warburg behavior related to the diffusion process throughout the ionically conductive domains made of SPE/CE/SPE or sole SPE, respectively. At 80 °C, the associated R_{dif} in the Li/OS/Oh/OS/Li cell of $312 \Omega \cdot \text{cm}^2$ is the double of the one in the Li/OS/Li cell ($153 \Omega \cdot \text{cm}^2$) within a 2% error margin. In addition, the characteristic times for the Li/OS/Li and Li/OS/Oh/OS/Li diffusion loops are very similar of 240.7 and 239.5 s, respectively. These characteristic times are proportional to the length of the diffusion gradient and the ambipolar diffusion coefficient,⁶² so the ionic diffusion process in the multilayered system is ascribed only to the two independent SPE layers surrounding the CE. In fact, the absence of a diffusive contribution from the Oh CE is expected as its t^+ is equal to 1. This situation depicted in Figure 4 is consistent with

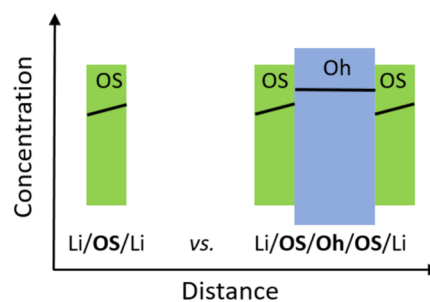


Figure 4. Scheme representing the steady-state concentration gradients formed across the respective electrolytes.

theoretical considerations published by Srinivasan et al.³³ Therefore, the limiting diffusion process in the multilayer composite electrolyte is due to the ionic diffusion in the SPE domains, which implies that (i) under the equilibrium condition, the kinetics of the ionic charge transfer at the SPE/CE interface is fast enough compared to mass transport kinetics to be considered as a reversible process, and (ii) when the thickness of the SPE is significantly reduced relative to that of the CE, the effective multilayer t^+ increases and tends to the t^+ of the CE. Indeed, assuming that Bruce and Vincent equations are valid,^{59,64,65} the transference number t^+ can be calculated according to eq 2 whose development from the Bruce–Vincent formula is detailed in the SI⁶⁶

$$t^+ = \frac{R_{\text{el}}}{R_{\text{el}} + R_{\text{dif}}} \quad (2)$$

Equation 2 can be converted to apply to the multilayer ($t^+_{\text{multilayer}}$) electrolytes based on R_{el_i} and R_{dif_j} where i corresponds to either the SPE or the CE material

$$t^+_{\text{multilayer}} = \frac{2R_{\text{el}_{\text{SPE}}} + R_{\text{el}_{\text{CE}}}}{2R_{\text{el}_{\text{SPE}}} + R_{\text{el}_{\text{CE}}} + 2R_{\text{dif}_{\text{SPE}}}} \quad (3)$$

Equation 3 can be rewritten using the geometry (thickness l_i) and physical properties (conductivity σ_i and Li^+ transference number t^+) of the SPE and CE materials

$$t_{\text{multilayer}}^+ = \frac{\frac{2l_{\text{SPE}}}{\sigma_{\text{SPE}}} + \frac{l_{\text{CE}}}{\sigma_{\text{CE}}}}{\frac{2l_{\text{SPE}}}{\sigma_{\text{SPE}}} + \frac{l_{\text{CE}}}{\sigma_{\text{CE}}} + \frac{2l_{\text{SPE}}(1-t_{\text{SPE}}^+)}{\sigma_{\text{SPE}} t_{\text{SPE}}^+}} \quad (4)$$

Using the previous realistic multilayer example of the two thin SPE layers having a t^+ of 0.2 (similar to a PEO electrolyte) sandwiching a thicker single-ion conducting CE, a transference number of 0.24 is calculated for the 22 μm thick multilayer. In the multilayer system, the matter transport kinetics corresponding to the ion migration (effective electrolyte conductivity at HF) and diffusion (LF) can be separately probed by EIS and can be predicted according to eqs 1 and 4, respectively. Therefore, the bulk transport properties are not modified by the interfacial ionic charge transfer probed in the MF range.

Finally, the MF loop of the multilayer symmetric cells (see Figures 1 and 2) enables the extraction of the SPE/CE interface contribution by the two different methodologies. The characteristic frequencies, located at the apex of the semicircle in the impedance spectra measured as a function of temperature by the two cell types (Li/Li vs SS/SS), are plotted in Arrhenius coordinates in Figure S7. The good agreement between the two sets of data all over the explored temperature range (between -20 and 100 $^\circ\text{C}$) confirms that the same phenomenon is probed in both cases. The Arrhenius plot of the Oh/OS interface resistance (R_{ct}) obtained from the two symmetric cell types is displayed in Figure 5 showing very similar R_{ct} values and activation energies from the slopes ($\chi^2 > 0.99$) with values of 0.85 eV and 0.84 eV for the blocking and nonblocking electrodes, respectively. This result means that for the realistic multilayer assembly used in the previous example, R_{ct} will be 100 and 25 times higher than R_{el} and $R_{\text{el}} + R_{\text{dif}}$ at 20 $^\circ\text{C}$, respectively. Thus, in the multilayer, the effective transport

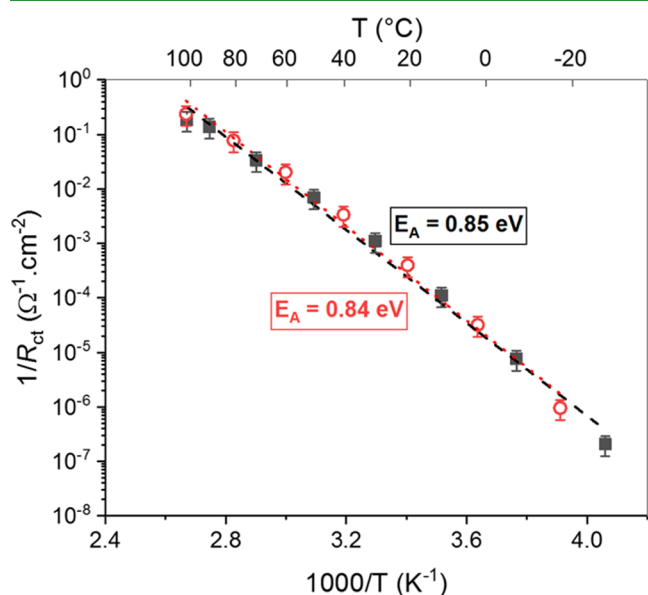


Figure 5. Arrhenius plots of the Oh/OS interfacial resistance obtained through a blocking electrode configuration (filled squares) from the cell SS/OS/Oh/OS/SS and a nonblocking electrode configuration (open circles) from the cell Li/OS/Oh/OS/Li.

properties can be drastically improved (eqs 1 and 4), but the overall polarization resistance, R_p (with $R_p = R_{\text{el}} + R_{\text{ct}} + R_{\text{dif}}$), depends mainly on R_{ct} i.e., to the ionic charge transfer at the SPE/CE interface. In practice, unless R_{ct} is very small (fast ionic charge transfer), composite electrolytes must be designed to limit the number of SPE/CE interfaces the Li^+ ions must cross. Moreover, by extrapolating this result to a well-dispersed composite electrolyte without CE grains percolation (typically $<30\%$ in volume), the effective conductivity due to ion migration measured at HF should not be affected by the interfacial ionic charge transfer occurring at MF.

To further understand the ionic charge transfer mechanism, the R_{ct} between Oh and PEO/LiTFSI- x M membranes was determined using blocking electrode cells. The PEO/Oh interfacial resistances are displayed in an Arrhenius plot in Figure 6a for the studied salt concentrations in between 70 and 100 $^\circ\text{C}$. For each concentration, a linear trend is obtained, indicating that R_{ct} is linked to a thermally activated charge transfer process that obeys an Arrhenius law. The activation energy (E_a) was then calculated from the slope of each curve in Figure 6a and is reported as a function of the salt concentration in Table S3. E_a is found to be independent of the salt concentration with an average value of 0.72 ± 0.03 eV, suggesting that the charge transfer mechanism is independent of salt concentration, in contrast to the results of Sagane et al.,³¹ where a slight increase in activation energy is measured with increasing salt concentration for the LLTO/PC-LiTFSI interface. Moreover, the Arrhenius trend of R_{ct} is also preserved at temperatures down to 10 $^\circ\text{C}$ as shown for the PEO/LiTFSI-0.6M SPE in Figure 6b, displaying R_{ct} and R_{SPE} (SPE bulk conductivity). This indicates that R_{ct} is not related to the PEO bulk crystallization (at about 60 $^\circ\text{C}$), as reported by Tenhaeff and co-workers.⁵⁵ For SPEs with a lower concentration, R_{ct} could not be properly extracted below 60 $^\circ\text{C}$ due to the low SPE conductivity inducing strong frequency superposition of the interfacial and bulk contributions. Interestingly, despite using a quite similar SPE/CE combination [PEO/LiCF₃SO₃ (EO/Li = 16, $x = 1.3$ M) and Oh], Chen et al.⁵⁰ observed a disruption in their Arrhenius plot of R_{ct} with an activation energy that doubles below the PEO melting temperature T_m (from 0.36 eV for $T > T_m$ up to 0.81 eV for $T < T_m$), while their R_{ct} values are similar to ours for $T > T_m$ ($42 \Omega\cdot\text{cm}^2$ at 70 $^\circ\text{C}$ compared to our value of $38 \Omega\cdot\text{cm}^2$ for PEO/LiTFSI-1.7M/Oh).

In the literature, to get a clearer view of the ionic charge transfer mechanism, the phenomenology of an electrochemical reaction governed by the Butler–Volmer equation occurring at an electrode interface has been adopted by Schleitner et al.³² and Brogioli et al.⁵⁷ to describe Li-ion transfer at LE/CE and an SPE/CE interface, respectively. Gondran et al.⁶⁷ proposed a Butler–Volmer-like kinetic law to model Na^+ -ion transfer at the SPE/CE interface. A similar model was adopted by Girault et al. to study the charge transfer between two immiscible liquids.⁶⁸ Herein, we assume a Butler–Volmer kinetic for the ionic charge transfer reaction according to



where Li_{SPE}^+ refers to Li^+ ions solvated inside the SPE and $[\text{Li}^+]_{\text{CE}}$ refers to sites occupied by Li^+ ions at the ceramic surface.

The exchange current density in the equilibrium can be written (see detailed calculation in the Supporting Information) as

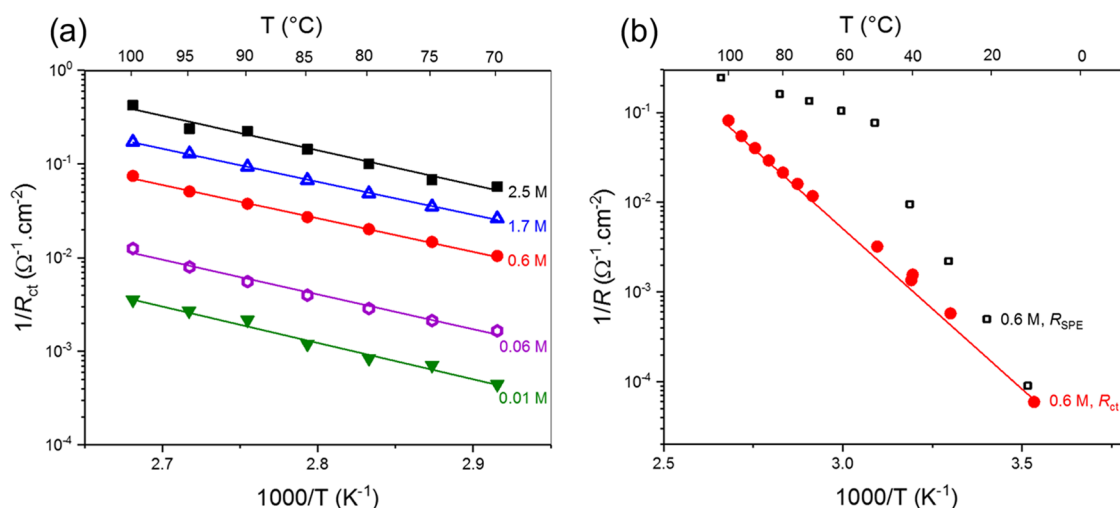


Figure 6. Arrhenius plots displaying $1/R$ versus $1000/T$ for (a) the interfacial charge transfer at the PEO/Oh interface at different LiTFSI concentrations for a temperature range of 100–70 °C and (b) comparison of the bulk PEO/LiTFSI-0.6M resistance (thickness of 102 μm) with charge transfer resistance at the PEO/LiTFSI-0.6M/Oh interface for a temperature range of 100–10 °C.

$$i_0 = FK^\circ C_{\text{Li}^+_{\text{SPE}}}^{(1-\alpha)} \quad (6)$$

with

$$K^\circ = k_1^\circ e^{-(\Delta_r G_{\text{SPE} \rightarrow \text{CE}})/RT} \quad (7)$$

where k_1° stands for the kinetic rate constant and $\Delta_r G_{\text{SPE} \rightarrow \text{CE}}$ stands for the free activation energy related to Li^+ charge transfer from the SPE to the CE. The activity coefficients are herein fixed to 1, simplifying the expression for K° compared to the one given in the SI. Finally, the interfacial charge transfer resistance R_{ct} is linked⁴³ to i_0 by a factor RT/F such as

$$R_{\text{ct}} = \frac{RT}{Fi_0} = \frac{RT}{F^2 * K^\circ C_{\text{Li}^+_{\text{SPE}}}^{(1-\alpha)}} \quad (8)$$

Consequently, R_{ct} is proportional to $C_{\text{Li}^+_{\text{SPE}}}^{-(1-\alpha)}$, i.e., theoretically the resistance will decrease with increasing Li^+ concentration in the polymer electrolyte according to a power law of exponent $-(1-\alpha)$. By drawing a parallel between this kinetic model and the Arrhenius behavior reported in Figure 6, the activation energies (listed in Table S3) refer to the enthalpic part of $\Delta_r G_{\text{SPE} \rightarrow \text{CE}}$, whereas its entropic term is embedded in the preexponential factor of eq S13. To validate the kinetic law presented here, we investigate the evolution of R_{ct} with the salt content (x).

Figure 7 displays in a log–log scale the isothermal evolutions of R_{ct} at the PEO/Oh interface as a function of the salt concentration, x , in between 70 and 100 °C. In this representation, R_{ct} decreases linearly with x for each temperature, indicating that the PEO/Oh interface obeys Butler–Volmer kinetics and the activity coefficient of Li^+ charge carrier in the SPE can be considered as constant and equal to 1 as there is no effect of charge carrier interactions even at a high concentration, supporting the simplification of eq S12 into eq 7. The linearity in Figure 7 also suggests that charge transfer is the dominant contribution for the interfacial resistance, and any other interface contributions (e.g., interphase) are small. In contrast, in the work of Brogioli et al.,⁵⁷ the dependence of R_{ct} of a PEO/LLZO:Al interface at 70 °C with PEO salt content, also displayed in Figure 7, presents first a -0.5 slope below 26 mM followed by a plateau value at a higher salt concentration.

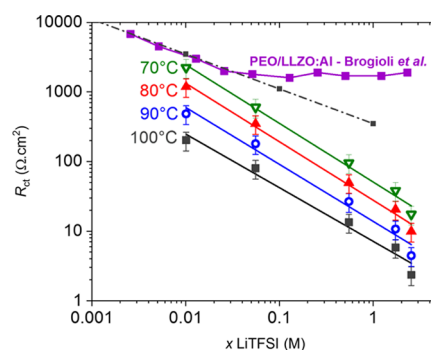


Figure 7. Variation of the PEO/Oh interface resistance at different salt concentrations for different temperatures from 70 to 100 °C. Literature values from Brogioli et al. at 70 °C are also included.⁵⁷ The dotted/dashed line represents a power law of -0.5 .

The authors attributed this transition regime to the presence of a space charge layer on either side of the interface between the organic and inorganic materials. In addition, for the EC:DMC:LiPF6/LLZO:Ta interface, Schleutker et al.³² reported a similar trend to Brogioli et al.,⁵⁷ but interpreted the transition regime as an additional interfacial resistance due to the presence of an interphase. Several groups have studied the influence of salt concentration on ionic charge transfer resistance between a ceramic and a liquid^{30–33} or an SPE.^{26,53,67} In their recent review, Janek et al.²⁵ highlighted a large variation of results in the R_{ct} salt dependence, which suggests that additional factors other than salt content are at stake. For example, Gupta et al.²⁶ reported a decrease in interfacial resistance at the PEO/LLZO:Ta interface with increasing LiTFSI concentration between 0.8 and 1.4 M. Above this concentration, an abrupt increase in R_{ct} was observed, assigned to salt precipitation at the ceramic surface hindering charge transfer. In the log–log plot in Figure 7, a straight line is observed with a gradient of -0.82 ± 0.03 (for all temperatures), suggesting that R_{ct} is a power law of the salt concentration, which is in accordance with the kinetic model (see eq 8). The symmetry factor α is therefore found equal to 0.18. Additionally, the exchange current density i_0 can be calculated from the R_{ct} values (see eq 8). For example, i_0 is

equal to $0.77 \pm 0.08 \text{ mA/cm}^2$ at $70 \text{ }^\circ\text{C}$ for the PEO/LiTFSI-1.7M/Oh, which is in the same order of magnitude as the one reported by Schleutker et al.³² and almost 13 times larger than that measured by Srinivasan et al.³³ for an Oh/EC:DEC (1:1)-LiPF₆-0.5M interface. From the symmetry factor α , the apparent kinetic constant K° (eq 8) at $20 \text{ }^\circ\text{C}$ of the PEO/LiTFSI-1.7M/Oh charge transfer reaction is $7.3 \pm 0.7 \times 10^{-5} \text{ M}^{-0.82} \cdot \text{s}^{-1}$, obtained from the y -intercept of $1/R_{\text{ct}}$ vs $1/T$. To the best of our knowledge, this is the first time an SPE/CE charge transfer kinetic constant is reported. Interestingly, the K° value is in the same order of magnitude as the one corresponding to Li⁺ intercalation into a LiMn₂O₄ electrode using PC as the electrolyte.⁶⁹

Another physical parameter of importance provided by the EIS analysis is the interfacial PEO/Oh capacitance (C_{ct}). In the electrical circuit in Figure 1c, the interfacial CPE_(SPE+CE) (of pseudocapacitance Q_{ct}) is in parallel with R_{ct} . An equivalent capacitance can be calculated according to

$$C_{\text{ct}} = Q_{\text{ct}}^{1/n} R_{\text{ct}}^{1-1/n} \quad (9)$$

with n being the exponent of the CPE.

The values of n , tabulated in Table S4, are always in the range of [0.85; 1], reflecting a good contact quality at the interface between the SPE and the CE. In addition, C_{ct} is displayed as a function of x in Figure 8 at 80 and $100 \text{ }^\circ\text{C}$. All

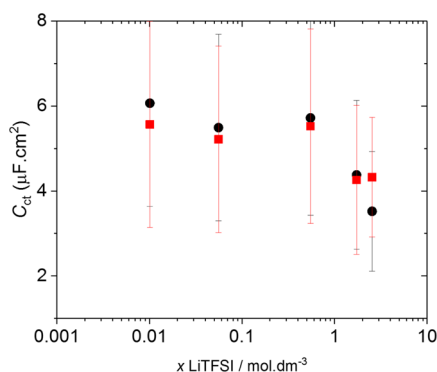


Figure 8. PEO/Oh interfacial capacitance at different concentrations of LiTFSI in the PEO. Circles and squares from data at 100 and $80 \text{ }^\circ\text{C}$, respectively.

over the concentration range, C_{ct} is constant with an average value of $5 \pm 2 \text{ } \mu\text{F/cm}^2$ independent of the temperature. This result is similar to the work of Gondran et al. on the NaSICON/PEO/NaI- x M interface⁶⁷ and the NaSICON/aqueous solution interface⁷⁰ with interfacial capacitance values in the range of $1 \text{ } \mu\text{F/cm}^2$. Considering that space charge layers are formed within the volume of both electrolytes on either side of the SPE/CE interface, the interfacial capacitance (C_{ct}) corresponds to the equivalent capacitance of two capacitances in series, i.e., one for the PEO side ($C_{\text{ct,PEO}}$) and another at the CE side ($C_{\text{ct,CE}}$); thus

$$\frac{1}{C_{\text{ct}}} = \frac{1}{C_{\text{ct,PEO}}} + \frac{1}{C_{\text{ct,CE}}} \quad (10)$$

The value of C_{ct} is therefore dominated by the contribution arising from the smallest capacitance. In our study, since the total capacity measured is found to be independent of the salt concentration in the polymer, the interfacial capacity that

dominates here is attributed to the one on the ceramic side in agreement with Gondran et al.⁶⁷

CONCLUSIONS

In this study, we use impedance spectroscopy to study the ionic transport in multilayers SPE/Oh/SPE, with PEO or PEO-based polymer OS and the NaSICON-type ceramic electrolyte Oh, using either SS blocking electrodes or reversible Li electrodes. The electrolyte resistance (HF part of the EIS spectrum) of the multilayer is found to be additive while the diffusion contribution (LF part) is determined by the polymer only, which confirms that the SPE/Oh interface is nonblocking, and the charge transfer at the interface is reversible. SPE/Oh interfacial resistances (MF part) determined using both SS (blocking) and Li (reversible) electrodes give coherent values, indicating that both methods can be used to extract the SPE/CE interface resistance and capacitance.

The PEO/Oh interface was subsequently probed using SS electrodes and a PEO/Oh/PEO multilayer, varying the LiTFSI concentration. The interfacial resistance R_{ct} is found to be inversely proportional to $C_{\text{Li}^+}^{0.82}$ over the studied concentration range, suggesting a nonsymmetrical Butler–Volmer-type charge transfer reaction with a constant activation energy of 0.72 eV . The interfacial capacitance value is also found independent of the PEO salt concentration, suggesting that the Oh ceramic capacitance is the dominating one.

Thus, in these types of multilayered system, the overall polarization resistance (R_p) can be fully decomposed by EIS methodology as being the sum of all of the resistive processes in the system such as the bulk migration resistance in the electrolytes (SPE and CE) R_{el} , the bulk ion diffusion resistance in the polymer electrolyte only R_{dif} and the ion transfer reaction resistance R_{ct} such that $R_p = R_{\text{el}} + R_{\text{ct}} + R_{\text{dif}}$. Simple algebraic equations (eqs 1 and 4) allow the calculation of the effective conductivity and transference number of the multilayer knowing the values for each layer SPE and CE. For R_p in multilayer systems to be minimized, future research should aim at minimizing R_{ct} , the largest contribution. To design an efficient multilayer system, many parameters must be taken into account, such as temperature, salt content, nature of the organic and inorganic electrolyte, as well as considering the underlying parameters that control R_{ct} , namely, ionic exchange current density, which depends on symmetry factor and apparent kinetic constant.

ASSOCIATED CONTENT

Supporting Information

The Supporting Information is available free of charge at <https://pubs.acs.org/doi/10.1021/acsami.1c19235>.

ICP-MS details for determining the salt concentration in each polymer membrane, additional Nyquist and Bode plots, conductivity of Oh measured by the subtraction methodology, DSC of the polymer OS, VTF fits and corresponding parameters, details on t^+ eq 2 derivation, characteristic frequencies of the OS/Oh interface contribution, conductivities of the PEO electrolytes and their corresponding multilayers, activation energies and n parameter (exponent of the CPE for the equivalence circuit) of the PEO/Oh interface, comparison of bulk conductivity and interfacial resistance of PEO/Oh, and details on the kinetic charge transfer model (PDF)

AUTHOR INFORMATION

Corresponding Author

Renaud Bouchet – Univ. Grenoble Alpes, Univ. Savoie Mont Blanc, CNRS, Grenoble INP, LEPMI, 38000 Grenoble, France; orcid.org/0000-0002-4040-2253; Email: renaud.bouchet@grenoble-inp.fr

Authors

James Alfred Isaac – Univ. Grenoble Alpes, Univ. Savoie Mont Blanc, CNRS, Grenoble INP, LEPMI, 38000 Grenoble, France; orcid.org/0000-0002-6692-114X

Léa Rose Mangani – Univ. Grenoble Alpes, Univ. Savoie Mont Blanc, CNRS, Grenoble INP, LEPMI, 38000 Grenoble, France; orcid.org/0000-0002-2608-8229

Didier Devaux – Univ. Grenoble Alpes, Univ. Savoie Mont Blanc, CNRS, Grenoble INP, LEPMI, 38000 Grenoble, France; orcid.org/0000-0002-1964-0556

Complete contact information is available at: <https://pubs.acs.org/10.1021/acsami.1c19235>

Author Contributions

[‡]J.A.I. and L.R.M. contributed equally to this work. R.B. designed the project. Experimental data were collected by L.R.M. and J.A.I. Data analysis and interpretation were performed by L.R.M. and J.A.I. with the help of R.B. and D.D. L.R.M. and J.A.I. wrote the article with the help of R.B. and D.D. All authors have given approval to the final version of the manuscript.

Funding

The Agence de la Transition Ecologique (ADEME) is acknowledged for the funding through the project IDOLES No. 1982C0016. In addition, the Association Nationale de la Recherche et de la Technologie (ANRT) and the company SAFT are also acknowledged for their financial support through contract no. 2019/1133.

Notes

The authors declare no competing financial interest.

ACKNOWLEDGMENTS

The authors thank Vincent Martin for help with the ICP-MS analysis of the polymer membranes.

REFERENCES

- Armand, M.; Tarascon, J. M. Issues and Challenges Facing Rechargeable Lithium Batteries. *Nature* **2001**, *414*, 359–367.
- Varzi, A.; Raccichini, R.; Scrosati, B. Challenges and Prospects of the Role of Solid Electrolytes in the Revitalization of Lithium Metal Batteries. *J. Mater. Chem. A* **2016**, *4*, 17251–17259.
- Niu, C.; Lee, H.; Chen, S.; Li, Q.; Du, J.; Xu, W.; Zhang, J. G.; Whittingham, M. S.; Xiao, J.; Liu, J. High-Energy Lithium Metal Pouch Cells with Limited Anode Swelling and Long Stable Cycles. *Nat. Energy* **2019**, *4*, 551–559.
- Xiang, Y.; Li, J.; Lei, J.; Liu, D.; Xie, Z.; Qu, D.; Li, K.; Deng, T.; Tang, H. Advanced Separators for Lithium-Ion and Lithium–Sulfur Batteries: A Review of Recent Progress. *ChemSusChem* **2016**, *9*, 3023–3039.
- Peled, E.; Menkin, S. Review—SEI: Past, Present and Future. *J. Electrochem. Soc.* **2017**, *164*, A1703–A1719.
- Zhang, J.; Cui, C.; Wang, P. F.; Li, Q.; Chen, L.; Han, F.; Jin, T.; Liu, S.; Choudhary, H.; Raghavan, S. R.; Eidson, N.; Cresce, A.; Ma, L.; Uddin, J.; Addison, D.; Yang, C.; Wang, C. “Water-in-Salt” Polymer Electrolyte for Li-Ion Batteries. *Energy Environ. Sci.* **2020**, *13*, 2878–2887.
- Wan, H.; Liu, S.; Deng, T.; Xu, J.; Zhang, J.; He, X.; Ji, X.; Yao, X.; Wang, C. Bifunctional Interphase-Enabled Li₁₀GeP₂S₁₂ Electrolytes for Lithium-Sulfur Battery. *ACS Energy Lett.* **2021**, *6*, 862–868.
- Tan, D. H. S.; Banerjee, A.; Chen, Z.; Meng, Y. S. From Nanoscale Interface Characterization to Sustainable Energy Storage Using All-Solid-State Batteries. *Nat. Nanotechnol.* **2020**, *15*, 170–180.
- Chen, R.; Li, Q.; Yu, X.; Chen, L.; Li, H. Approaching Practically Accessible Solid-State Batteries: Stability Issues Related to Solid Electrolytes and Interfaces. *Chem. Rev.* **2019**, *120*, 6820–6877.
- Long, L.; Wang, S.; Xiao, M.; Meng, Y. Polymer Electrolytes for Lithium Polymer Batteries. *J. Mater. Chem. A* **2016**, *4*, 10038–10069.
- Zhou, D.; Shanmukaraj, D.; Tkacheva, A.; Armand, M.; Wang, G. Polymer Electrolytes for Lithium-Based Batteries: Advances and Prospects. *Chem* **2019**, *5*, 2326–2352.
- Wang, C.; Zhang, H.; Dong, S.; Hu, Z.; Hu, R.; Guo, Z.; Wang, T.; Cui, G.; Chen, L. High Polymerization Conversion and Stable High-Voltage Chemistry Underpinning an In Situ Formed Solid Electrolyte. *Chem. Mater.* **2020**, *32*, 9167–9175.
- Sun, C.; Liu, J.; Gong, Y.; Wilkinson, D. P.; Zhang, J. Recent Advances in All-Solid-State Rechargeable Lithium Batteries. *Nano Energy* **2017**, *33*, 363–386.
- Meesala, Y.; Jena, A.; Chang, H.; Liu, R. S. Recent Advancements in Li-Ion Conductors for All-Solid-State Li-Ion Batteries. *ACS Energy Lett.* **2017**, *2*, 2734–2751.
- Keller, M.; Varzi, A.; Passerini, S. Hybrid Electrolytes for Lithium Metal Batteries. *J. Power Sources* **2018**, *392*, 206–225.
- Fu, X.; Yu, D.; Zhou, J.; Li, S.; Gao, X.; Han, Y.; Qi, P.; Feng, X.; Wang, B. Inorganic and Organic Hybrid Solid Electrolytes for Lithium-Ion Batteries. *CrystEngComm* **2016**, *18*, 4236–4258.
- Ju, J.; Wang, Y.; Chen, B.; Ma, J.; Dong, S.; Chai, J.; Qu, H.; Cui, L.; Wu, X.; Cui, G. Integrated Interface Strategy toward Room Temperature Solid-State Lithium Batteries. *ACS Appl. Mater. Interfaces* **2018**, *10*, 13588–13597.
- Chen, L.; Li, Y.; Li, S. P.; Fan, L. Z.; Nan, C. W.; Goodenough, J. B. PEO/Garnet Composite Electrolytes for Solid-State Lithium Batteries: From “Ceramic-in-Polymer” to “Polymer-in-Ceramic”. *Nano Energy* **2018**, *46*, 176–184.
- Keller, M.; Appetecchi, G. B.; Kim, G. T.; Sharova, V.; Schneider, M.; Schuhmacher, J.; Roters, A.; Passerini, S. Electrochemical Performance of a Solvent-Free Hybrid Ceramic-Polymer Electrolyte Based on Li₇La₃Zr₂O₁₂ in P(EO)15LiTFSI. *J. Power Sources* **2017**, *353*, 287–297.
- Langer, F.; Bardenhagen, I.; Glenneberg, J.; Kun, R. Microstructure and Temperature Dependent Lithium Ion Transport of Ceramic-Polymer Composite Electrolyte for Solid-State Lithium Ion Batteries Based on Garnet-Type Li₇La₃Zr₂O₁₂. *Solid State Ionics* **2016**, *291*, 8–13.
- Guo, Q.; Han, Y.; Wang, H.; Xiong, S.; Li, Y.; Liu, S.; Xie, K. New Class of LAGP-Based Solid Polymer Composite Electrolyte for Efficient and Safe Solid-State Lithium Batteries. *ACS Appl. Mater. Interfaces* **2017**, *9*, 41837–41844.
- Bae, J.; Li, Y.; Zhang, J.; Zhou, X.; Zhao, F.; Shi, Y.; Goodenough, J. B.; Yu, G. A 3D Nanostructured Hydrogel-Framework-Derived High-Performance Composite Polymer Lithium-Ion Electrolyte. *Angew. Chem., Int. Ed.* **2018**, *57*, 2096–2100.
- Jayasekara, I.; Poyner, M.; Teeters, D. Investigation of a Nanoconfined, Ceramic Composite, Solid Polymer Electrolyte. *Electrochim. Acta* **2017**, *247*, 1147–1154.
- Li, S.; Zhang, S.; Shen, L.; Liu, Q.; Ma, J.; Lv, W.; He, Y.; Yang, Q. Progress and Perspective of Ceramic/Polymer Composite Solid Electrolytes for Lithium Batteries. *Adv. Sci.* **2020**, *7*, No. 1903088.
- Weiss, M.; Simon, F. J.; Busche, M. R.; Nakamura, T.; Schröder, D.; Richter, F. H.; Janek, J. From Liquid-to Solid-State Batteries: Ion Transfer Kinetics of Heteroionic Interfaces. *Electrochem. Energy Rev.* **2020**, *3*, 231–238.
- Gupta, A. *Analyzing the Stability and Kinetics of Ceramic Electrolyte/Organic Electrolyte Interfaces for Li Metal Batteries*; University of Michigan, 2020.

- (27) Kuhnert, E.; Ladenstein, L.; Jodlbauer, A.; Slugovc, C.; Trimmel, G.; Wilkening, H. M. R.; Rettenwander, D. Lowering the Interfacial Resistance in Li_{6.4}La₃Zr_{1.4}Ta_{0.6}O₁₂/Poly(Ethylene Oxide) Composite Electrolytes. *Cell Rep. Phys. Sci.* **2020**, *1*, No. 100214.
- (28) Jow, T. R.; Delp, S. A.; Allen, J. L.; Jones, J.-P.; Smart, M. C. Factors Limiting Li + Charge Transfer Kinetics in Li-Ion Batteries. *J. Electrochem. Soc.* **2018**, *165*, A361–A367.
- (29) Ishihara, Y.; Miyazaki, K.; Fukutsuka, T.; Abe, T. Kinetics of Lithium-Ion Transfer at the Interface between Li₄Ti₅O₁₂ Thin Films and Organic Electrolytes. *ECS Electrochem. Lett.* **2014**, *3*, A83–A86.
- (30) Abe, T.; Sagane, F.; Ohtsuka, M.; Iriyama, Y.; Ogumi, Z. Lithium-Ion Transfer at the Interface between Lithium-Ion Conductive Ceramic Electrolyte and Liquid Electrolyte—a Key to Enhancing the Rate Capability of Lithium-Ion Batteries. *J. Electrochem. Soc.* **2005**, *152*, 2151–2154.
- (31) Sagane, F.; Abe, T.; Ogumi, Z. Li⁺-Ion Transfer through the Interface between Li⁺-Ion Conductive Ceramic Electrolyte and Li⁺-Ion-Concentrated Propylene Carbonate Solution. *J. Phys. Chem. C* **2009**, *113*, 20135–20138.
- (32) Schleitker, M.; Bahner, J.; Tsai, C. L.; Stolten, D.; Korte, C. On the Interfacial Charge Transfer between Solid and Liquid Li⁺ Electrolytes. *Phys. Chem. Chem. Phys.* **2017**, *19*, 26596–26605.
- (33) Mehrotra, A.; Ross, P. N.; Srinivasan, V. Quantifying Polarization Losses in an Organic Liquid Electrolyte/Single Ion Conductor Interface. *J. Electrochem. Soc.* **2014**, *161*, A1681–A1690.
- (34) Pham, Q. N.; Bohnke, O.; Bohnke, C. Potentiometric Measurements and Impedance Characteristics of Li_{0.30}La_{0.57}Ti_{0.3}O₃ Membrane in Lithium Anhydrous Solutions. *Electrochim. Acta* **2006**, *51*, 6186–6193.
- (35) Sagane, F.; Miyazaki, K.; Fukutsuka, T.; Iriyama, Y.; Abe, T.; Ogumi, Z. Lithium-Ion Transfer at the Interface between Solid and Liquid Electrolytes under Applying DC Voltage. *Chem. Lett.* **2010**, *39*, 826–827.
- (36) Busche, M. R.; Drossel, T.; Leichtweiss, T.; Weber, D. A.; Falk, M.; Schneider, M.; Reich, M. L.; Sommer, H.; Adelhelm, P.; Janek, J. Dynamic Formation of a Solid-Liquid Electrolyte Interphase and Its Consequences for Hybrid-Battery Concepts. *Nat. Chem.* **2016**, *8*, 426–434.
- (37) Busche, M. R.; Leichtweiss, T.; Fiedler, C.; Drossel, T.; Geiss, M.; Weiß, M.; Kronenberger, A.; Dominik, W.; Janek, J. The Formation of the Solid-/Liquid Electrolyte Interphase (SLEI) on NASICON-Type Glass Ceramics and LiPON. *Adv. Mater. Interfaces* **2020**, *7*, No. 2000380.
- (38) Yamada, Y.; Sagane, F.; Iriyama, Y.; Abe, T.; Ogumi, Z. Kinetics of Lithium-Ion Transfer at the Interface between Li_{0.35}La_{0.55}Ti_{0.3}O₃ and Binary Electrolytes. *J. Phys. Chem. C* **2009**, *113*, 14528–14532.
- (39) Sagane, F.; Abe, T.; Iriyama, Y.; Ogumi, Z. Li⁺ and Na⁺ Transfer through Interfaces between Inorganic Solid Electrolytes and Polymer or Liquid Electrolytes. *J. Power Sources* **2005**, *146*, 749–752.
- (40) Sagane, F.; Abe, T.; Ogumi, Z. Sodium-Ion Transfer at the Interface between Ceramic and Organic Electrolytes. *J. Power Sources* **2010**, *195*, 7466–7470.
- (41) Sagane, F.; Abe, T.; Ogumi, Z. Electrochemical Analysis of Lithium-Ion Transfer Reaction through the Interface between Ceramic Electrolyte and Ionic Liquids. *J. Electrochem. Soc.* **2012**, *159*, No. A1766.
- (42) Liu, J.; Gao, X.; Hartley, G. O.; Rees, G. J.; Gong, C.; Richter, F. H.; Janek, J.; Xia, Y.; Robertson, A. W.; Johnson, L. R.; Bruce, P. G. The Interface between Li_{6.5}La₃Zr_{1.5}Ta_{0.5}O₁₂ and Liquid Electrolyte. *Joule* **2020**, *4*, 101–108.
- (43) Bard, A. J.; Faulkner, L. R. *Electrochemical Methods: Fundamentals and Applications*, 2nd ed.; Harris, D.; Swain, E.; Robey, C.; Aiello, E., Eds.; John Wiley & Sons, Inc., 2001.
- (44) Vetter, K. J. *Electrochemical Kinetics, Theoretical and Experimental Aspects*; Academic Press: New York, 1967.
- (45) Hamann, H.; Vielstich, W. *Elektrochemie II—Elektrodenprozesse, Angewandte Elektrochemie*; Verlag Chemie: Weinheim, 1981.
- (46) Gondran, C.; Siebert, E.; Fabry, P. Internal Reference System Based on Poly(Ethylene Oxide) Networks. *Sens. Actuators, B* **1997**, *44*, 554–558.
- (47) Riphhaus, N.; Stiaszny, B.; Beyer, H.; Indris, S.; Gasteiger, H. A.; Sedlmaier, S. J. Understanding Chemical Stability Issues between Different Solid Electrolytes in All-Solid-State Batteries. *J. Electrochem. Soc.* **2019**, *166*, A975–A983.
- (48) Nairn, K. M.; Best, A. S.; Newman, P. J.; MacFarlane, D. R.; Forsyth, M.; et al. Ceramic-Polymer Interface in Composite Electrolytes of Lithium Aluminum Titanium Phosphate and Polyetherurethane Polymer Electrolyte. *Solid State Ionics* **1999**, *121*, 115–119.
- (49) Tenhaeff, W. E.; Perry, K. A.; Dudney, N. J. Impedance Characterization of Li Ion Transport at the Interface between Laminated Ceramic and Polymeric Electrolytes. *J. Electrochem. Soc.* **2012**, *159*, 2118–2123.
- (50) Chen, X. C.; Liu, X.; Samuthira Pandian, A.; Lou, K.; Delnick, F. M.; Dudney, N. J. Determining and Minimizing Resistance for Ion Transport at the Polymer/Ceramic Electrolyte Interface. *ACS Energy Lett.* **2019**, *4*, 1080–1085.
- (51) Langer, F.; Palagonia, M. S.; Bardenhagen, I.; Glenneberg, J.; La Mantia, F.; Kun, R. Impedance Spectroscopy Analysis of the Lithium Ion Transport through the Li₇La₃Zr₂O₁₂/P(EO)₂₀Li Interface. *J. Electrochem. Soc.* **2017**, *164*, A2298–A2303.
- (52) Simon, F. J.; Hanauer, M.; Henss, A.; Richter, F. H.; Janek, J. Properties of the Interphase Formed between Argyrodite-Type Li₆PS₅Cl and Polymer-Based PEO₁₀:LiTFSI. *ACS Appl. Mater. Interfaces* **2019**, *11*, 42186–42196.
- (53) Gupta, A.; Sakamoto, J. Controlling Ionic Transport through the PEO-LiTFSI/LLZTO Interface. *Electrochem. Soc. Interface* **2019**, *28*, 63–69.
- (54) Abe, T.; Ohtsuka, M.; Sagane, F.; Iriyama, Y.; Ogumi, Z. Lithium Ion Transfer at the Interface between Lithium-Ion-Conductive Solid Crystalline Electrolyte and Polymer Electrolyte. *J. Electrochem. Soc.* **2004**, *151*, 1950–1953.
- (55) Tenhaeff, W. E.; Yu, X.; Hong, K.; Perry, K. A.; Dudney, N. J. Ionic Transport across Interfaces of Solid Glass and Polymer Electrolytes for Lithium Ion Batteries. *J. Electrochem. Soc.* **2011**, *158*, No. A1143.
- (56) Simon, F. J.; Hanauer, M.; Richter, F. H.; Janek, J. Interphase Formation of PEO₂₀:LiTFSI-Li₆PS₅Cl Composite Electrolytes with Lithium Metal. *ACS Appl. Mater. Interfaces* **2020**, *12*, 11713–11723.
- (57) Brogioli, D.; Langer, F.; Kun, R.; La Mantia, F. Space-Charge Effects at the Li₇La₃Zr₂O₁₂/Poly(Ethylene Oxide) Interface. *ACS Appl. Mater. Interfaces* **2019**, *11*, 11999–12007.
- (58) Osaka Soda, 2020. <http://www.osaka-soda.co.jp/en/prd/index.html>.
- (59) Devaux, D.; Bouchet, R.; Glé, D.; Denoyel, R. Mechanism of Ion Transport in PEO/LiTFSI Complexes: Effect of Temperature, Molecular Weight and End Groups. *Solid State Ionics* **2012**, *227*, 119–127.
- (60) OHARA Corporation. Ohara, 2020. <https://www.oharacorp.com>.
- (61) Banerjee, A.; Wang, X.; Fang, C.; Wu, E. A.; Meng, Y. S. Interfaces and Interphases in All-Solid-State Batteries with Inorganic Solid Electrolytes. *Chem. Rev.* **2020**, *120*, 6878–6933.
- (62) Bouchet, R.; Lascaud, S.; Rosso, M. An EIS Study of the Anode Li/PEO-LiTFSI of a Li Polymer Battery. *J. Electrochem. Soc.* **2003**, *150*, 1385–1389.
- (63) Aziz, S. B.; Woo, T. J.; Kadir, M. F. Z.; Ahmed, H. M. A. Conceptual Review on Polymer Electrolytes and Ion Transport Models. *J. Sci.: Adv. Mater. Devices* **2018**, *3*, 1–17.
- (64) Bruce, P.; Evans, J.; Vincent, C. A. Conductivity and Transference Number Measurements on Polymer Electrolytes. *Solid State Ionics* **1988**, *28–30*, 918–922.
- (65) Watanabe, M.; Nagano, S.; Sanui, K.; Ogata, N. Estimation of Li⁺ Transport Number in Polymer Electrolytes by the Combination of Complex Impedance and Potentiostatic Polarization Measurements. *Solid State Ionics* **1988**, *28–30*, 911–917.

(66) Wohde, F.; Balabajew, M.; Roling, B. Li + Transference Numbers in Liquid Electrolytes Obtained by Very-Low-Frequency Impedance Spectroscopy at Variable Electrode Distances. *J. Electrochem. Soc.* **2016**, *163*, A714–A721.

(67) Gondran, C.; Albert, F.; Siebert, E. Kinetics of Sodium and Silver Exchange on a PEO-NaI-AgI. *Soild State Ionics* **1996**, *84*, 131–138.

(68) Girault, H. H. The Potential Dependence of the Rate of Ion Transfer Reactions across a Liquid/Liquid Interface. *J. Electroanal. Chem.* **1988**, *257*, 47–55.

(69) Vassiliev, S. Y.; Sentyurin, V. V.; Levin, E. E.; Nikitina, V. A. Diagnostics of Lithium-Ion Intercalation Rate-Determining Step: Distinguishing between Slow Desolvation and Slow Charge Transfer. *Electrochim. Acta* **2019**, *302*, 316–326.

(70) Mauvy, F.; Gondran, C.; Siebert, E. Potentiometric Selectivity and Impedance Characteristics of a NASICON-Based Ion Selective Electrode. *Electrochim. Acta* **1999**, *44*, 2219–2226.